J. Fluid Mech. (2011), *vol.* 688, *pp.* 66–87.
doi:10.1017/jfm.2011.365

Motion of slender bodies in unsteady Stokes flow

Efrath Barta†

Bar-Code Computers Ltd, Tirat-HaCarmel, 39120, Israel

(Received 14 December 2010; revised 22 August 2011; accepted 30 August 2011;
first published online 13 October 2011)

The flow regime in the vicinity of oscillatory slender bodies, either an isolated one or a row of many bodies, immersed in viscous fluid (i.e. under creeping flow conditions) is studied. Applying the slender-body theory by distributing proper singularities on the bodies' major axes yields reasonably accurate and easily computed solutions. The effect of the oscillations is revealed by comparisons with known Stokes flow solutions and is found to be most significant for motion along the normal direction. Streamline patterns associated with motion of a single body are characterized by formation and evolution of eddies. The motion of adjacent bodies results, with a reduction or an increase of the drag force exerted by each body depending on the direction of motion and the specific geometrical set-up. This dependence is demonstrated by parametric results for frequency of oscillations, number of bodies, their slenderness ratio and the spacing between them. Our method, being valid for a wide range of parameter values and for densely packed arrays of rods, enables simulation of realistic flapping of bristled wings of some tiny insects and of locomotion of flagella and ciliated micro-organisms, and might serve as an efficient tool in the design of minuscule vehicles. Its potency is demonstrated by a solution for the flapping of thrips.

Key words: Low-Reynolds-number flows, slender-body theory

1. Introduction

The relative ease with which the Stokes equations can be handled has made problems of motion in Stokes flow an appealing and well-known field of research for more than 150 years. In the 'classic' Stokes flow, the basic assumptions are: (*a*) the Reynolds number (*Re*) is sufficiently small that only viscous terms are retained in the complete Navier–Stokes equations, and (*b*) the motion is in steady-state, and hence temporal derivatives are omitted. The mathematical solutions of the equations were proposed to describe and explain many forms of feeding and locomotion in the zoological realm, from ciliary motion, described by Gray as early as in 1928 (Gray 1928), to insect flight dealt with by Weihs and Barta in 2008 (Weihs & Barta 2008). While serving as milestones in the qualitative description of motion of flagella and cilia (but not in the quantitative description of 'wave-like' motion of ciliated surfaces; see Brennen & Winet 1977), those time-independent solutions are inadequate models for flapping wings and hovering insects since time-averaged approaches are not sufficient to address questions relating to flight control (Dudley 2000; Taylor 2001); or,

† Email address for correspondence: efrathb@gmail.com

as Ellington (1984) stated, the unsteady effects have an increased significance in the hovering of insects. Indeed, when trying to apply steady-state solutions to simulations of the flight of insects belonging to the thrips family (described by Sunada *et al.* 2002), the steady-state solution (Barta & Weihs 2006) failed to balance the computed force related to the motion of the wings and the weight of the insect (Barta & Weihs 2004). The typical eddies found in the vicinity of oscillatory bodies, which are absent when eliminating the time factor from the equations, are another aspect of the qualitative differences between steady and unsteady situations, which considerably affect the motion of small particles near the moving body, and prohibit the steady solutions from accurately simulating the feeding of swimming micro-organisms or the sensing of signals contained in movements of surrounding air by the thin hairs that cover insects and spiders (Bathellier *et al.* 2005). Hence the importance of time-dependent solutions. From a non-dimensionalization of the Navier–Stokes equations it is clear that, when the particle displacement is very small compared to its characteristic size, linearization of the equations (i.e. retaining the time derivative while omitting the inertial–convective term) is justified. Such situations are typical of the flows produced by the swimming of microscopic organisms (Pozrikidis 1989*a*) and of the dynamics of arachnid and insect filiform hairs (Bathellier *et al.* 2005), and occur in the design of extremely small flying vehicles (Zussman, Yarin & Weihs 2002) and in electroacoustics (where the particle motion is merely ultrasonic buzzing, Loewenberg 1994).

Solutions for the unsteady, three-dimensional Stokes flow (represented by the linearized Navier–Stokes equations) are known for a sphere (Stokes 1851), for the axisymmetric motion of spheroids with aspect ratios in the range of $[0.1, 10]$ (Lawrence & Weinbaum 1988), for cylinders (Loewenberg 1994), and for dumbbells and biconcave disks (Pozrikidis 1989*b*). These solutions are found (*a*) by implementing perturbation methods, in which case they are valid only for very low or very high frequencies of oscillations (e.g. Smith 1997, who solved for the oscillatory flow past a circular cylinder when the frequency tends to zero), (*b*) by solving for the streamfunction, in which case they can address only axisymmetric cases (e.g. Lawrence & Weinbaum 1986), or (*c*) by implementing boundary integral methods that involve intensive computational resources (e.g. Pozrikidis 1989*a*,*b*; Kohr 2003; D'Elía *et al.* 2010). This state of affairs has led us to seek for a method that will be sufficiently general, i.e. valid for a wide scope of frequencies and geometrical parameter values, but at the same time detailed, i.e. will yield not just global properties, such as the total force involved in the motion, but locally induced velocity fields too. It should be accurate and easy to implement in order to quantitatively simulate the detailed flow field for a wide range of situations from the laboratory or the zoological realm. Here we solve for the flow field around a moving elongated isolated body (as a potential model for the locomotion of flagella) and for the flow induced by an array of elongated bodies in viscous fluid (a configuration that might describe bristled wings composed of slender 'rods', as is common in the wings of insects, the locomotion of ciliated cells, eukaryote propulsion and the hairy legs of spiders and insects).

For the general, multi-body, steady-state situation the most obvious approach is to solve by distributing singularities either on the surface of the body (e.g. Kim & Karrila 1991) or along its axis – an appealing option, since it involves line integrals and not surface ones. Johnson (1980) was the first to formulate a method of axial distribution for the steady flow in a way that is both rigorous and uniformly valid over the surface of a slender body. In this method, the velocity induced by an axial distribution of

singularities is equated to the given velocity of the body to yield integral equations for the intensities of the singularities. The uniform asymptotic expansion of the integrands enables the conversion of the original equations to the easy-to-manipulate and stable Fredholm equations of the second kind. Barta & Liron (1988) extended this method so as to apply it to two bodies, and Barta & Weihs (2006) further extended it for a finite row of slender bodies in close proximity.

Dealing with the unsteady case necessitates distribution of appropriate fundamental solutions. Tsai *et al.* (2006) used a space–time unification method and complicated expressions for the fundamental solutions in their solution for a general time-dependent Stokes flow. A major simplification is achieved when one uses the fact that any given time-dependent velocity (and pressure) field might be described by its harmonics, i.e. represented by its Fourier series. Due to the linearity of the involved equations, this actually means that any velocity field is a combination of fields that are invoked by oscillatory motions. Pozrikidis (1989*a*) has defined the Stokeslet, doublet and rotlet for oscillatory motion in viscous flow. Shatz (2004) has defined higher-order singularities. Both used distribution of singularities (Pozrikidis on the surface of the body and Shatz on its axis) in order to solve for the motion of spheroids with aspect ratios in the range of $[0.1, 10]$ that oscillate with low to moderate frequencies.

Here we apply slender-body theory to spheroids with very small aspect ratio and determine the ratio between the Stokeslets' and doublets' intensities, which enables an accurate and uniformly valid solution. First, we solve for an isolated body: these solutions are relevant for the motion of flagellar propulsion. The equations are given in § 2 along with numerical solutions, parametric investigations and analysis of the results. Streamlines that characterize the motion and demonstrate local features are drawn and global properties are found by computation of the total drag force. Note that although we write here the equations for spheroids, our method is applicable for any slender body possibly with a curved major axis (see Barta & Liron 1988). Therefore it may simulate the hydromechanics of flagella with planar waves, as described by Brennen & Winet (1977), as long as its motion does not involve considerable stretching or contraction. Next, in § 3, we solve for two and then a row of oscillating spheroids, in order to elucidate the effect of a body on its neighbours. Conclusions regarding the efficacy of the clustering of the bodies, shown to be highly dependent on the direction of motion, are drawn based on both locally induced velocities and the total force exerted by the bodies. A specific simulation of the flapping of an insect is given in § 4 and the meaning and implications of this work are discussed in § 5.

2. An isolated slender spheroid in oscillatory Stokes flow

We consider oscillatory flow in an unbounded domain. Thus the velocity and pressure are given by $\boldsymbol{U} = \boldsymbol{u}\exp(-\mathrm{i}\omega t)$ and $P = p\exp(-\mathrm{i}\omega t)$, where ω is the frequency of the oscillations. Inserting these expressions into the linearized Navier–Stokes equations and non-dimensionalizing all variables yields the following momentum equation:

$$\lambda^2\boldsymbol{u} = -\boldsymbol{\nabla}p + \nabla^2\boldsymbol{u}, \tag{2.1}$$

where $\lambda^2 = -\mathrm{i}\omega dl^2/\nu$, dl is a typical length of the problem (usually chosen as the radius of the body in the direction perpendicular to the motion) and ν is the kinematic viscosity of the fluid. Equation (2.1), combined with the continuity equation, $\boldsymbol{\nabla}\cdot\boldsymbol{u} = 0$, and with no-slip conditions at the surface of the involved body, uniquely determines

the flow field for any oscillatory motion, and therefore for any field whose time-dependence can be expressed by a Fourier series.

The fundamental solutions of the above equations are given in Pozrikidis (1989*a*). The velocity at point x induced by a Stokeslet with intensity vector $\boldsymbol{\alpha}$ situated at point y is

$$u_i = \frac{1}{8\pi}\left(\frac{A(R)\delta_{ij}}{r} + \frac{B(R)r_i r_j}{r^3}\right)\alpha_j, \quad i,j = 1,2,3, \tag{2.2}$$

where $\boldsymbol{r}$ is the vector that connects x and y, $r = |\boldsymbol{r}|$, $R = \lambda r$ and

$$A(R) = 2\mathrm{e}^{-R}\left(1 + \frac{1}{R} + \frac{1}{R^2}\right) - \frac{2}{R^2}, \tag{2.3}$$

$$B(R) = -2\mathrm{e}^{-R}\left(1 + \frac{3}{R} + \frac{3}{R^2}\right) + \frac{6}{R^2}. \tag{2.4}$$

The velocity at point x induced by a doublet with intensity vector $\boldsymbol{\beta}$ situated at point y is

$$u_i = \frac{1}{8\pi}\left(\frac{C(R)\delta_{ij}}{r^3} - \frac{3D(R)r_i r_j}{r^5}\right)\beta_j, \quad i,j = 1,2,3, \tag{2.5}$$

where

$$C(R) = \mathrm{e}^{-R}(1 + R + R^2), \tag{2.6}$$

$$D(R) = \mathrm{e}^{-R}(1 + R + R^2/3). \tag{2.7}$$

2.1. *The governing equations*

Following slender-body theory, a slender spheroid of revolution is represented by a distribution of singularities along its major axis between its foci. To leading order, only Stokeslets (2.2), (2.3) and (2.4) and doublets (2.5), (2.6) and (2.7) are considered. Due to the linearity of the equations, every motion is given as a combination of motions along three orthogonal directions, here chosen to coincide with the body's coordinate system: tangential (t), normal (n) and bi-normal (b) to the body's major axis.

In a pioneering work, Johnson (1980) used a uniformly valid asymptotic expansion (inner plus outer expansions minus inner–outer expansion), and by analytical considerations found that in order to have a constant velocity on the circumference of the body, the ratio between the doublet intensity at point s on the axis, $\boldsymbol{\beta}(s)$, and the Stokeslet intensity there, $\boldsymbol{\alpha}(s)$, should be $\beta_j(s) = (\varepsilon^2/2)(e^2 - s^2)\alpha_j(s)$, $j = t, n, b$, where ε is the slenderness ratio of the spheroid and $\pm e$ its foci: $e^2 = 1 - \varepsilon^2$ (length normalization is done with respect to half the body length l). This choice enabled the formulation of integral equations that were accurate to within an error of $O(\varepsilon/\ln\varepsilon)$. The same ratio was determined for the case of multiple bodies (Barta & Liron 1988; Barta & Weihs 2006).

Here, the situation is more complicated since the above 'classical' ratio is not justified, as is proved below. Using inner, outer and inner–outer expansions of the distances between a point situated at the cross-sectional plane, at height s, with ψ as its circumferential angle, and the singularities that are distributed on the axis of the body, one gets the following expressions for the velocity components at the surface of the body, u (along either the normal or bi-normal direction) and v (along the

tangential direction):

$$
\begin{aligned}
u(s,\psi) = &\int_{-e}^{e} \frac{(\alpha_n(s') - \alpha_n(s))A(\lambda|s'-s|)}{|s'-s|}\,\mathrm{d}s' \\
&+ \int_{-(e+s)/\varepsilon}^{(e-s)/\varepsilon} \frac{\alpha_n(s)A(\lambda\varepsilon\sqrt{\sigma^2+(1-s^2)})}{\sqrt{\sigma^2+(1-s^2)}} \\
&+ \frac{\beta_n(s)C(\lambda\varepsilon\sqrt{\sigma^2+(1-s^2)})}{\varepsilon^2\sqrt{\sigma^2+(1-s^2)}^3}\,\mathrm{d}\sigma \\
&+ (1-s^2)\cos^2\psi \int_{-(e+s)/\varepsilon}^{(e-s)/\varepsilon} \frac{\alpha_n(s)B(\lambda\varepsilon\sqrt{\sigma^2+(1-s^2)})}{\sqrt{\sigma^2+(1-s^2)}^3} \\
&- \frac{3\beta_n(s)D(\lambda\varepsilon\sqrt{\sigma^2+(1-s^2)})}{\varepsilon^2\sqrt{\sigma^2+(1-s^2)}^5}\,\mathrm{d}\sigma, \qquad (2.8)
\end{aligned}
$$

$$
\begin{aligned}
v(s,\psi) = &\int_{-e}^{e} \frac{(\alpha_t(s') - \alpha_t(s))(A(\lambda|s'-s|)+B(\lambda|s'-s|))}{|s'-s|}\,\mathrm{d}s' \\
&+ \alpha_t(s) \int_{-(e+s)/\varepsilon}^{(e-s)/\varepsilon} \frac{A(\lambda\varepsilon\sqrt{\sigma^2+(1-s^2)})}{\sqrt{\sigma^2+(1-s^2)}} \\
&+ \frac{B(\lambda\varepsilon\sqrt{\sigma^2+(1-s^2)})\sigma^2}{\sqrt{\sigma^2+(1-s^2)}^3}\,\mathrm{d}\sigma \\
&+ \frac{\beta_t(s)}{\varepsilon^2} \int_{-(e+s)/\varepsilon}^{(e-s)/\varepsilon} \frac{C(\lambda\varepsilon\sqrt{\sigma^2+(1-s^2)})}{\sqrt{\sigma^2+(1-s^2)}^3} \\
&- \frac{3D(\lambda\varepsilon\sqrt{\sigma^2+(1-s^2)})\sigma^2}{\sqrt{\sigma^2+(1-s^2)}^5}\,\mathrm{d}\sigma. \qquad (2.9)
\end{aligned}
$$

The above equations were derived by retaining only the leading-order terms in the asymptotic expansion of the distances involved (the details appear in the appendix of Johnson 1980) and in the functions A, B, C, D. When the argument $R = \lambda r$ is large, all these functions have a constant, zero value, so any approximation of the argument will do. When $R = \lambda r$ is small, due to the continuity of all the functions, the leading term of their argument is the relevant argument (and the order of magnitude of the errors made by omitting smaller terms is not altered by those functions remaining the same as in the steady-state solutions).

It is clear that in order to get a uniform velocity on the surface of the spheroid, the ψ-dependent term (the third integral) in (2.8) must be null. An attempt to nullify it by assuming that the doublets' intensities are constant within the region of integration (and thus could be taken out of the integral sign) will lead to highly inaccurate solutions, as was found for the steady-state case. Thus, one has to assume a relation of the form $\beta_j(s) = \varepsilon^2(e^2 - s^2)\gamma_j(s)$ for any direction j (doublet strength is always proportional to the cross-sectional radius squared, but the proportionality constant $\gamma(s)$ may vary along the axis), and substitute it in the above equations to get the correct

relation between the intensities of the singularities:

$$\beta_j(s) = \frac{\alpha_j(s)\varepsilon^2(e^2 - s^2)}{3} \times \frac{\displaystyle\int_{-(e+s)/\varepsilon}^{(e-s)/\varepsilon} \frac{B(\lambda\varepsilon\sqrt{\sigma^2 + (1-s^2)})}{\sqrt{\sigma^2 + (1-s^2)}^3}\,\mathrm{d}\sigma}{\displaystyle\int_{-(e+s)/\varepsilon}^{(e-s)/\varepsilon} \frac{(e^2 - (s-\varepsilon\sigma)^2)D(\lambda\varepsilon\sqrt{\sigma^2 + (1-s^2)})}{\sqrt{\sigma^2 + (1-s^2)}^5}\,\mathrm{d}\sigma}. \tag{2.10}$$

Note that relation (2.10) above depends on λ, and thus the relation between the Stokeslets and doublets here is not just a function of geometry, as is the case in the steady-state solution, but of the frequency of the oscillations too. Clarke *et al.* (2006) solved for a slender cylinder near a wall by distributing transient Stokeslets (2.2), (2.3) and (2.4) and steady-state doublets with the steady-state ratio between the frequencies. Therefore their work is valid only for low frequencies. As long as $\lambda\varepsilon$ is much smaller than 1 (for then the functions B and D reach their asymptotic value of 1), using the steady-state relation between the intensities does not hamper the solution, but dealing with higher frequencies requires implementation of (2.10).

By following the guidelines that lead to the formulation of the 'classic' ratio for the steady-state case (Johnson 1980), the reader may verify that (2.10) holds for any body with circular transverse cross-sections whose radius satisfies the equation $r = \varepsilon\sqrt{1 - s^2}$, and not just for slender spheroids.

Substitution of a given body velocity in (2.8) and (2.9) yields integral equations for $\alpha_n(s)$ and $\alpha_t(s)$, the Stokeslets intensities.

2.2. *Numerical solutions*

The decoupled equations (2.8) and (2.9), being Fredholm of the second type, are easily solved: we replace the integrals by sums according to the rectangle midpoint rule, get a system of linear algebraic equations for the intensities of the Stokeslets that are scattered along the body axis, and then solve by LU decomposition, using the Mathematica software by Wolfram Research. We successfully implemented our method for a very wide range of parameter values (slenderness ratios in the range 0.1–0.001 and frequency parameter from zero to a few hundred). It is found that representing half of the spheroid axis by 30 points is sufficient, i.e. it yields results that are much smaller than the asymptotic errors. This is verified in two ways: (*a*) *a posteriori*, by validating that the no-slip condition for the velocity is satisfied within an error no higher than that expected from the asymptotic expansions, and (*b*) by verifying that further refinement of the numerical mesh will not significantly change the results.

In order to unravel the effect of the unsteadiness on the solution, we compared the varying, complex-valued intensities found here to the constant Stokeslet intensity that characterizes the motion of a spheroid in Stokes flow determined by Chwang & Wu (1975). It turns out that the steepest variations of the intensities occur near the body's ends; see figures 1 and 2.

By comparing figures 1 and 2 it becomes clear that the effect of the oscillations is more pronounced when the motion is normal to the long axis. In every direction the phase attains its maximum absolute value at the centre and is diminished towards the foci, indicating that viscous characteristics (represented by the real part of the intensities) are more important at the body's ends than at its centre (in accordance with the findings of Pozrikidis 1989*a*).

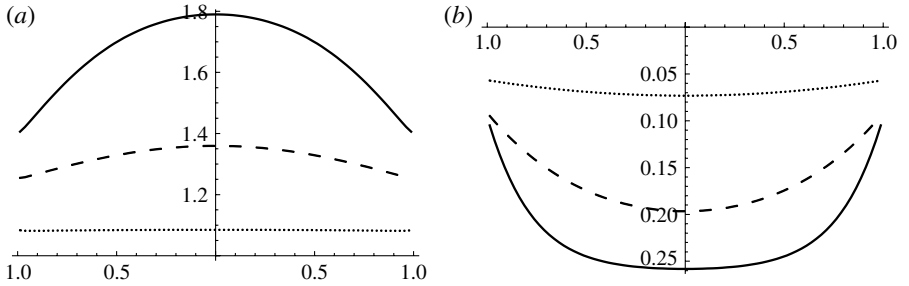

FIGURE 1. Distribution of the intensities of the oscillating Stokeslets along the axis of a slender spheroid with $\varepsilon = 0.01$ for various λ values: $|\lambda| = 0.5$ (dotted line), 2 (dashed line), 5 (solid line). Motion is along the normal direction. (*a*) Magnitude normalized by the value of the steady-state Stokeslet. (*b*) Phase.

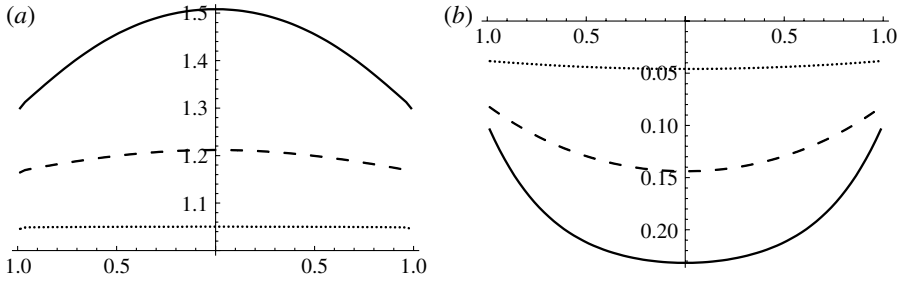

FIGURE 2. Distribution of the intensities of the oscillating Stokeslets along the axis of a slender spheroid with $\varepsilon = 0.01$ for various λ values: $|\lambda| = 0.5$ (dotted line), 2 (dashed line), 5 (solid line). Motion is along the tangential (axial) direction. (*a*) Magnitude normalized by the value of the steady-state Stokeslet. (*b*) Phase.

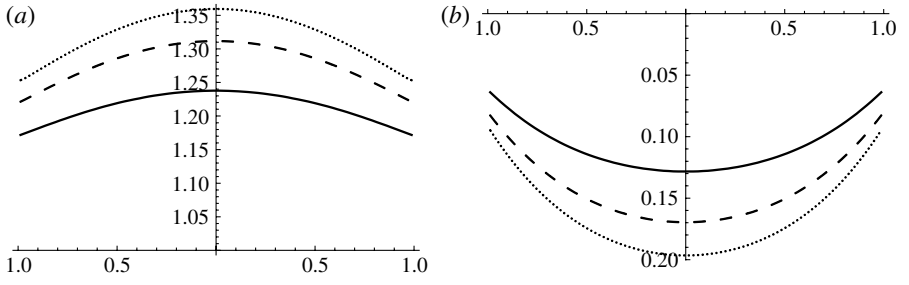

FIGURE 3. Distribution of the intensities of the oscillating Stokeslets along the axis of a slender spheroid: $|\lambda| = 2$: $\varepsilon = 0.01$ (dotted line), 0.005 (dashed line), 0.001 (solid line). Motion is along the normal direction. (*a*) Magnitude normalized by the value of the steady-state Stokeslet. (*b*) Phase.

Figures 3 and 4 demonstrate the effect of the slenderness ratio of the spheroid on the singularities' intensities: as the body becomes more slender, the effect of the oscillations is less pronounced.

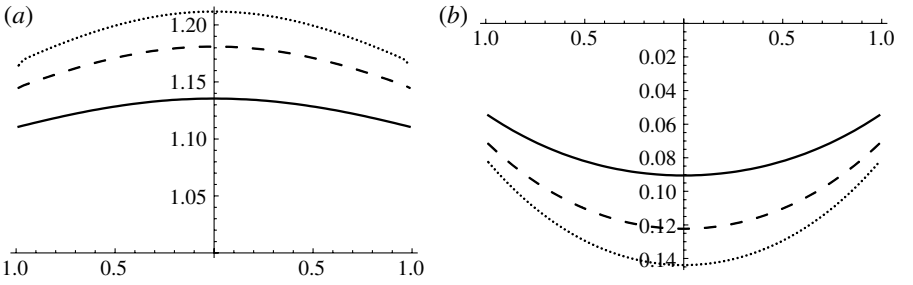

FIGURE 4. Distribution of the intensities of the oscillating Stokeslets along the axis of a slender spheroid: $|\lambda| = 2$; $\varepsilon = 0.01$ (dotted line), 0.005 (dashed line), 0.001 (solid line). Motion is along the tangential (axial) direction. (*a*) Magnitude normalized by the value of the steady-state Stokeslet. (*b*) Phase.

2.2.1. *The local flow field*

Due to the numerical simplicity of our method, it is easy to demonstrate the instantaneous evolution of the flow field around the body. The velocity at any arbitrary point is computed by integrating the velocities induced by all the distributed Stokeslets and doublets according to (2.2) and (2.5). Figures 5 and 6 present instantaneous streamline patterns for the flow around a spheroid with slenderness ratio $\varepsilon = 0.01$ and where $|\lambda| = 2$. Qualitatively, the patterns are the same as those plotted by Pozrikidis (1989*b*) for non-slender spheroids: namely, there is a generation, expansion and then disappearance of viscous eddies near the body. As expected, when $\omega t = \pi$ there is a reversal of the flow and the direction of motion alternates between sequential eddies. The higher the frequency of the oscillations the more 'irregular' is the instantaneous flow field, and eddies will be formed in the vicinity of the body. In motion normal to the axis the eddies are generated near the body's ends, while in axial motion the contour of the eddy conforms to the contour of the body.

2.2.2. *Drag force*

The total drag (per unit length) involved with the motion of a spheroid that moves in the *i*th direction with a unit velocity is given by (see Pozrikidis 1989*a*)

$$D_i = 8\pi \left(\mu \int_{-e}^{e} \alpha_i(s)\, \mathrm{d}s - (\lambda\varepsilon)^2 /6 \right) \quad i = t, n, b. \tag{2.11}$$

In table 1 we demonstrate the effect of the oscillations on the drag exerted by a spheroid that moves along any one of its axes for two slenderness ratios. In general, increasing the frequency of the oscillations increases the drag force, both its absolute value (magnitude) and its argument (phase). The effect is more pronounced when the body is less slender (ε is higher) and moves normal to its major axis; thus the ratio D_n/D_t increases with λ and asymptotically reaches a value of two, characteristic of potential flow.

Table 1 shows that for low frequencies (when the viscous effects are the important ones), ε has a minor effect on the magnitude of the drag, while for high frequencies ε has a tremendous effect – in accordance with the high sensitivity with respect to shape that is characteristic of potential flows (when the inertial effects are the important ones).

Lawrence & Weinbaum (1988) concluded that the dominance of a certain component of the total drag (steady Stokes flow resistance, non-dissipative added

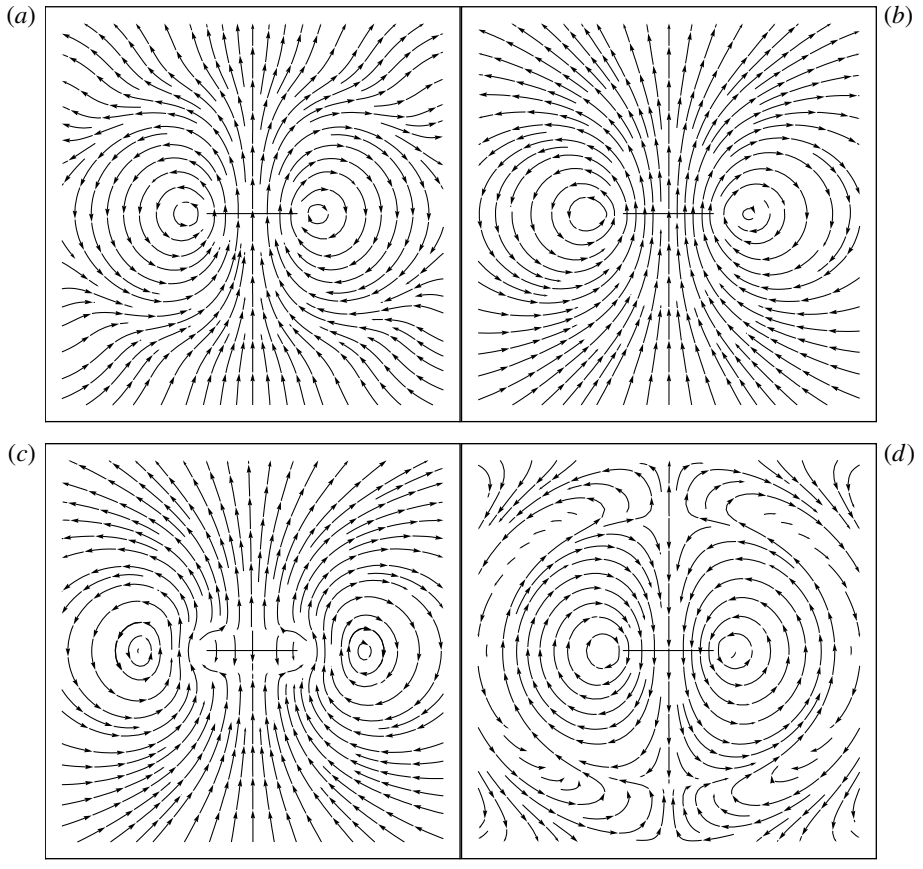

FIGURE 5. Instantaneous streamlines in the flow field around a slender spheroid that moves along the normal direction: $\varepsilon = 0.01$; $|\lambda| = 2$. (The spheroid is represented by the solid line at the centre.) (*a*) $\omega t = 0$; (*b*) $\omega t = 1$; (*c*) $\omega t = 2$; (*d*) $\omega t = 3$.

λ	$\varepsilon = 0.0025$		$\varepsilon = 0.01$	
	D_n	D_t	D_n	D_t
0	3.50	2.03	4.34	2.62
$(1-\mathrm{i})$	$4.14\mathrm{e}^{-0.11\mathrm{i}}$	$2.25\mathrm{e}^{-0.07\mathrm{i}}$	$5.35\mathrm{e}^{-0.14\mathrm{i}}$	$2.99\mathrm{e}^{-0.10\mathrm{i}}$
$3(1-\mathrm{i})$	$5.01\mathrm{e}^{-0.16\mathrm{i}}$	$2.60\mathrm{e}^{-0.13\mathrm{i}}$	$6.87\mathrm{e}^{-0.22\mathrm{i}}$	$3.62\mathrm{e}^{-0.18\mathrm{i}}$
$6(1-\mathrm{i})$	$5.81\mathrm{e}^{-0.18\mathrm{i}}$	$2.96\mathrm{e}^{-0.17\mathrm{i}}$	$8.46\mathrm{e}^{-0.27\mathrm{i}}$	$4.35\mathrm{e}^{-0.24\mathrm{i}}$
$10(1-\mathrm{i})$	$6.58\mathrm{e}^{-0.21\mathrm{i}}$	$3.33\mathrm{e}^{-0.20\mathrm{i}}$	$10.16\mathrm{e}^{-0.31\mathrm{i}}$	$5.16\mathrm{e}^{-0.29\mathrm{i}}$
$15(1-\mathrm{i})$	$7.35\mathrm{e}^{-0.23\mathrm{i}}$	$3.70\mathrm{e}^{-0.22\mathrm{i}}$	$12.02\mathrm{e}^{-0.36\mathrm{i}}$	$6.05\mathrm{e}^{-0.34\mathrm{i}}$

TABLE 1. The total drag exerted by a slender spheroid in oscillatory motion along its two axes.

mass force, Basset force, memory integral force) is a function of the aspect ratio and the frequency. In accordance with them, we found that the transition from viscous to inertial dominance for a motion in a given direction depends to leading order on $(|\lambda|\varepsilon)$ and to a lesser extent on ε. This is another demonstration of our previously stated

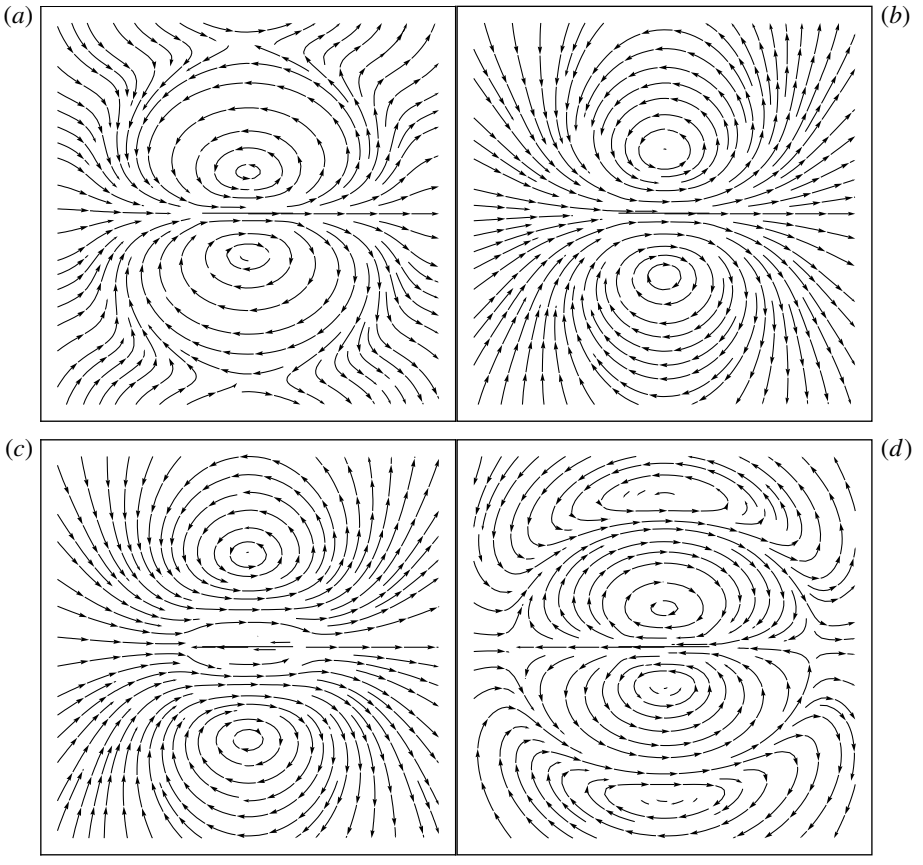

FIGURE 6. Instantaneous streamlines in the flow field around a slender spheroid that moves along the axial direction: $\varepsilon = 0.01$; $|\lambda| = 2$. (The spheroid is represented by the solid line at the centre.) (*a*) $\omega t = 0$; (*b*) $\omega t = 1$; (*c*) $\omega t = 2$; (*d*) $\omega t = 3$.

conclusion that the transient Stokes flow is more adequately approximated by the steady Stokes flow for extremely slender bodies, because where ε is very small, even for relatively high $|\lambda|$ values, the viscous effects are dominant. It is especially true for axial motion as the balance between the inertial forces and the viscous ones occurs at $|\lambda|\varepsilon \sim 1.6$ for transverse motion and at $|\lambda|\varepsilon \sim 15$ for axial motion (a lower value characterizes spheroids that are not very slender). Pozrikidis (1989*a*), dealing with non-slender spheroids (ε is close to 1) and normalizing with respect to the body width (thus 'translating' his findings into our terms means replacing $|\lambda|$ by $|\lambda|\varepsilon$), claimed that the inertial effects balance the viscous ones at $|\lambda| \sim 5$ and become dominant at $|\lambda| \sim 100$ for any aspect ratio. In another paper (Pozrikidis 1989*b*) he stated that this 'transition point' depends on the direction of the flow/motion.

2.3. *Varying velocities along the body axis*

Our method can be implemented not only for basic, constant oscillatory transition of a spheroid. Motions of a body in shear flow, paraboloidal flow, etc., can be solved by the same method of solution, but the expressions become quite lengthy as they involve the distribution of other types of singularities, such as rotlets, stresslets and quadrupoles, which are determined by taking the appropriate derivatives of the Stokeslet, (2.2), (2.3)

λ	$\varepsilon = 0.0025$	$\varepsilon = 0.01$
$1 - \mathrm{i}$	e	e
$5(1 - \mathrm{i})$	0.91	0.77
$15(1 - \mathrm{i})$	0.77	0.69
$50(1 - \mathrm{i})$	0.71	0.55

TABLE 2. Location, s, of the maximum of $|\alpha_n(s)|$ along the axis of a slender spheroid in oscillatory linearly increasing motion: $u(s) = 1 + s$, $s \in [-e, e]$ at $\omega t = 0$.

and (2.4). The ratio between the intensities of those singularities is formulated along the same lines that lead to (2.10): namely, they are always proportional to the cross-sectional radius squared or raised to the fourth power (depending on the specific order of the singularity), multiplied by appropriate quotients of lengthy integrals that depend on the frequency. However, there is another simple case that does not involve higher singularities and potentially has practical applications and meaning: a solution for a slender body that has a linearly increasing velocity in the normal direction. This might simulate a beat of a cilium that is fixed at one of its ends (i.e. it is attached to a larger body). Implementing (2.8) and (2.9) for a velocity vector that is a function of the location s on the body axis yields the solution. In a steady Stokes flow such a situation involves the distribution of Stokeslets that are found to have monotonically increasing intensities, (Barta & Liron 1988; Weihs & Barta 2008). Here, the variation of the intensities depends on both the slope of the varying velocity and the frequency of the oscillations. High frequencies involve maximum intensity at the centre of the body while low ones involve maximum intensity at the fast-moving end. Moderate values involve maximum intensity somewhere between those locations, as demonstrated in table 2. As found for the simpler cases above, the more slender the spheroid, the less important is the role played by the unsteadiness, and thus highly slender bodies are characterized by maximum intensity attained close to the fast-moving end.

Although the total drag involved with such motion remains the same as in the constant translation as long as the mean velocity of the spheroid remains unchanged, the local effects might be quite different, as is revealed by a comparison of figure 7 with figure 5.

One has to be cautious when applying our method to a cilium attached to a body, because the distribution of singularities without reflections with respect to the body means that the necessary no-slip conditions are not met on the body surface. However, by computing the velocity induced by those singularities, one may *a posteriori* estimate the inaccuracy of the solution. Due to the zero velocity at the end of the cilium that is fixed to the body, the Stokeslet intensities near the body are necessarily very small, thus inducing negligible velocity there. Indeed, when we computed the velocity induced by the spheroid described in figure 7, we found that the maximal induced velocity on a plane attached to the fixed end is within the limits of the accuracy of the equations; in other words, for all practical purposes the no-slip condition on the body is satisfied. Therefore, as a crude first approximation, one may implement our method for an elongated cilium or flagellum attached to a large body.

The linear increase of velocity is only an example for a beating cilium, but other variations are known to exist. For example, in their classic paper Blake & Sleigh (1974) claimed that the velocities at the first quarter of the cilium are very small for

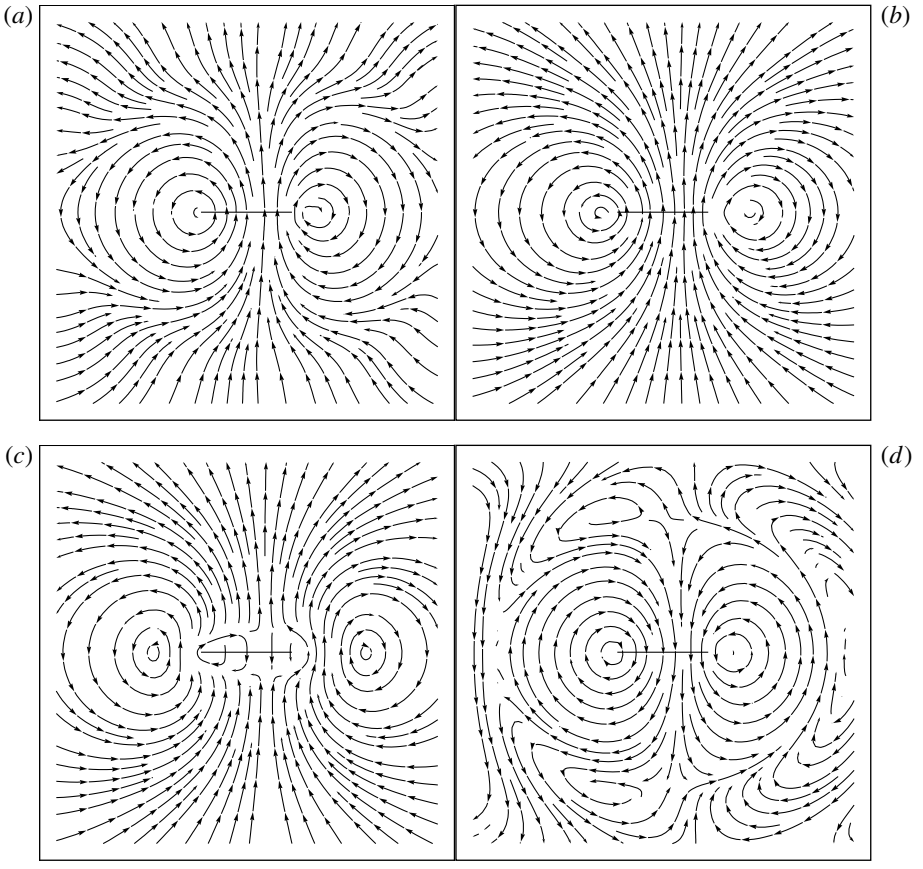

FIGURE 7. Instantaneous streamlines in the flow field around a slender spheroid that moves along the normal direction with linearly increasing motion: $u(s) = 1 + s$, $s \in [-e, e]$; $\varepsilon = 0.01$; $|\lambda| = 2$. (The spheroid is represented by the solid line at the centre.) (*a*) $\omega t = 0$; (*b*) $\omega t = 1$; (*c*) $\omega t = 2$; (*d*) $\omega t = 3$.

Opalina, *Paramecium* and *Pleurobrachia*, after that there is a steep increase, and at the fifth of the cilium that is far from the body the velocity profile flattens out – a situation that can be successfully handled by our approach.

3. A row of slender spheroids in oscillatory Stokes flow

We describe the flow field induced by the oscillatory motion of a finite row of parallel, slender spheroids immersed in an unbounded incompressible fluid. The spacing, d, between two adjacent spheroids satisfies $1 > d > 2\varepsilon$, and the number of rods, m, can be any integer from 2 upwards, limited only by computation time.

3.1. *The governing equations*

For each spheroid in the row ($i = 1, \ldots, m$) we write the equations for the three components of the velocity u, v, w (normal, tangential and bi-normal respectively) obtained by distribution of oscillatory Stokeslets and doublets along the major axes of each spheroid within the row where the ratio between the intensities is determined by using (2.10). Since this ratio was found to be satisfactory for the isolated spheroid, it is valid here as well, because the terms that are dependent on the azimuthal angle

(the ones that limit the accuracy of the solution) stem from the inner expansion of the equations, which remains unchanged in this case as the presence of the adjacent spheroids affects just the outer and inner–outer expansions. Thus

$$
\begin{aligned}
u^i(s) = &\int_{-e}^{e} \frac{(\alpha_n^i(s') - \alpha_n^i(s))A(\lambda|s'-s|)}{|s'-s|}\,\mathrm{d}s' \\
&+ \int_{-(e+s)/\varepsilon}^{(e-s)/\varepsilon} \frac{\alpha_n^i(s)A(\lambda\varepsilon\sqrt{\sigma^2+(1-s^2)})}{\sqrt{\sigma^2+(1-s^2)}} \\
&+ \frac{\gamma_n^i(s)(e^2-(s-\varepsilon\sigma)^2)C(\lambda\varepsilon\sqrt{\sigma^2+(1-s^2)})}{\sqrt{\sigma^2+(1-s^2)}^3}\,\mathrm{d}\sigma \\
&+ \sum_{\substack{j=1,\\ j\neq i}}^{m} \int_{-e}^{e} \frac{\alpha_n^j(s')A(\lambda\sqrt{(s-s')^2+(d(i-j))^2})}{\sqrt{(s-s')^2+(d(i-j))^2}}\,\mathrm{d}s' \\
&+ \varepsilon^2 \sum_{\substack{j=1,\\ j\neq i}}^{m} \int_{-e}^{e} \frac{\gamma_n^j(s')(e^2-s'^2)C(\lambda\sqrt{(s-s')^2+(d(i-j))^2})}{\sqrt{(s-s')^2+(d(i-j))^2}^3}\,\mathrm{d}s', \qquad (3.1)
\end{aligned}
$$

$$
\begin{aligned}
v^i(s) = &\int_{-e}^{e} \frac{(\alpha_t^i(s') - \alpha_t^i(s))(A(\lambda|s'-s|) + B(\lambda|s'-s|))}{|s'-s|}\,\mathrm{d}s' \\
&+ \alpha_t^i(s) \int_{-(e+s)/\varepsilon}^{(e-s)/\varepsilon} \frac{A(\lambda\varepsilon\sqrt{\sigma^2+(1-s^2)})}{\sqrt{\sigma^2+(1-s^2)}} + \frac{B(\lambda\varepsilon\sqrt{\sigma^2+(1-s^2)})\sigma^2}{\sqrt{\sigma^2+(1-s^2)}^3}\,\mathrm{d}\sigma \\
&+ \gamma_t^i(s) \int_{-(e+s)/\varepsilon}^{(e-s)/\varepsilon} (e^2-(s-\varepsilon\sigma)^2) \left(\frac{C(\lambda\varepsilon\sqrt{\sigma^2+(1-s^2)})}{\sqrt{\sigma^2+(1-s^2)}^3} \right. \\
&\left. - \frac{3D(\lambda\varepsilon\sqrt{\sigma^2+(1-s^2)})\sigma^2}{\sqrt{\sigma^2+(1-s^2)}^5} \right) \mathrm{d}\sigma \\
&+ \sum_{\substack{j=1,\\ j\neq i}}^{m} \int_{-e}^{e} \alpha_t^j(s') \left\{ \frac{A(\lambda\sqrt{(s-s')^2+(d(i-j))^2})}{\sqrt{(s-s')^2+(d(i-j))^2}} \right. \\
&\left. + \frac{(s-s')^2 B(\lambda\sqrt{(s-s')^2+(d(i-j))^2})}{\sqrt{(s-s')^2+(d(i-j))^2}^3} \right\} \mathrm{d}s' \\
&+ \sum_{\substack{j=1,\\ j\neq i}}^{m} \int_{-e}^{e} \gamma_t^j(s') \left\{ \frac{C(\lambda\sqrt{(s-s')^2+(d(i-j))^2})}{\sqrt{(s-s')^2+(d(i-j))^2}^3} \right. \\
&\left. - \frac{3(s-s')^2 D(\lambda\sqrt{(s-s')^2+(d(i-j))^2})}{\sqrt{(s-s')^2+(d(i-j))^2}^5} \right\} \varepsilon^2(e^2-s'^2)\,\mathrm{d}s' \\
&+ \sum_{\substack{j=1,\\ j\neq i}}^{m} \left\{ \int_{-e}^{e} \alpha_b^j(s') \frac{B(\lambda\sqrt{(s-s')^2+(d(i-j))^2})}{\sqrt{(s-s')^2+(d(i-j))^2}^3} \right.
\end{aligned}
$$

$$- \gamma_b^j(s') \frac{3\varepsilon^2(e^2 - s'^2) D(\lambda\sqrt{(s-s')^2 + (d(i-j))^2})}{\sqrt{(s-s')^2 + (d(i-j))^2}^5} \times d(i-j)(s-s')\,\mathrm{d}s', \tag{3.2}$$

$$\begin{aligned} w^i(s) = & \int_{-e}^{e} \frac{(\alpha_b^i(s') - \alpha_b^i(s)) A(\lambda|s'-s|)}{|s'-s|}\,\mathrm{d}s' \\ & + \int_{-(e+s)/\varepsilon}^{(e-s)/\varepsilon} \frac{\alpha_b^i(s) A(\lambda\varepsilon\sqrt{\sigma^2 + (1-s^2)})}{\sqrt{\sigma^2 + (1-s^2)}} \\ & + \frac{\gamma_b^i(s)(e^2 - (s - \varepsilon\sigma)^2) C(\lambda\varepsilon\sqrt{\sigma^2 + (1-s^2)})}{\sqrt{\sigma^2 + (1-s^2)}^3}\,\mathrm{d}\sigma \\ & + \sum_{\substack{j=1,\\ j\neq i}}^{m} \int_{-e}^{e} \alpha_b^j(s') \left\{ \frac{A(\lambda\sqrt{(s-s')^2 + (d(i-j))^2})}{\sqrt{(s-s')^2 + (d(i-j))^2}} \right. \\ & \left. + \frac{d^2 (i-j)^2 B(\lambda\sqrt{(s-s')^2 + (d(i-j))^2})}{\sqrt{(s-s')^2 + (d(i-j))^2}^3} \right\} \mathrm{d}s' \\ & + \sum_{\substack{j=1,\\ j\neq i}}^{m} \int_{-e}^{e} \gamma_b^j(s') \left\{ \frac{C(\lambda\sqrt{(s-s')^2 + (d(i-j))^2})}{\sqrt{(s-s')^2 + (d(i-j))^2}^3} \right. \\ & \left. - \frac{3d^2 (i-j)^2 D(\lambda\sqrt{(s-s')^2 + (d(i-j))^2})}{\sqrt{(s-s')^2 + (d(i-j))^2}^5} \right\} \varepsilon^2(e^2 - s'^2)\,\mathrm{d}s' \\ & + \sum_{\substack{j=1,\\ j\neq i}}^{m} \int_{-e}^{e} \left\{ \frac{\alpha_t^j(s') B(\lambda\sqrt{(s-s')^2 + (d(i-j))^2})}{\sqrt{(s-s')^2 + (d(i-j))^2}^3} \right. \\ & \left. - \frac{3\varepsilon^2(e^2 - s'^2)\gamma_t^j(s') D(\lambda\sqrt{(s-s')^2 + (d(i-j))^2})}{\sqrt{(s-s')^2 + (d(i-j))^2}^5} \right\} \\ & \times d(i-j)(s-s')\,\mathrm{d}s'. \end{aligned} \tag{3.3}$$

The solution of the above system of $3m$ integral equations, (3.1), (3.2) and (3.3), with the ratio specified in (2.10) that defines $\gamma(s)$, yields the Stokeslet intensities $\alpha_n^i(s)$, $\alpha_t^i(s)$, $\alpha_b^i(s)$.

3.2. *Numerical solutions*

The method of solution used for the isolated body applies here too. Motion along the normal direction is decoupled from motion along any one of the other directions, and thus solving for motion along the e_n direction involves a solution of mn linear equations (n being the number of discrete points scattered along each spheroid axis) while solving for motion along either the e_t or e_b directions involves $2mn$ linear equations. Since most of the computational work is done in the process of determination of the coefficients of the equations, a solution for one of these two directions yields a solution for the other direction with redundant additional

computational effort. Symmetry, either around the centre of the bodies or around the centre of the row, halves the original number of equations.

3.2.1. *Two parallel spheroids*

The significant effect of the interaction between two spheroids in Stokes flow, even when the distance between the bodies is considerable, was determined long ago both numerically (Barta & Liron 1988) and experimentally (e.g. Cheer & Koehl 1987). When one body moves, it drags the surrounding viscous fluid where the other body is immersed, thus helping it to move in the same direction and reducing the total drag involved with the motion. The reduction is most significant in motion along the axis that 'connects' the bodies (the bi-normal direction) and least significant in motion along the spheroid axis (the tangential direction).

In oscillatory motion the situation is qualitatively different due to the presence of the inertial forces in addition to the viscous effects. As Feng & Joseph (1995) found, a boundary close to a moving body enhances the effect of the unsteadiness on the flow field, indicating that an assumption of a 'classical' Stokes flow in a system of two bodies might be unjustified more than it is for an isolated body.

As is demonstrated by figure 8, low frequencies of oscillations induce flow fields that are quite similar to typical Stokes flow, i.e. the two bodies drag and 'help' each other even when the distance between them is large, especially in motion in the bi-normal direction. However, high frequencies cause the viscous effects to be inferior to the inertial effects to the extent that, in some cases, the presence of the other body disturbs and hinders the motion (i.e. requires exertion of higher drag force). For axial motion the effect of the other body's presence is moderate. For transverse motion, however, if it is in the normal direction, then the moderate help of the other body (due to viscosity) is overridden by its interference (due to inertia), but for the motion in the bi-normal direction, the profound help of the other body overrides the inertial interference unless the frequency of oscillations is very high. Some combinations of frequency and spacing between the bodies lead to situations where the presence of another body hardly affects the motion due to a near-balance between the help of viscous forces and the interference of inertial forces. As was found for the steady-state situation, the more slender the spheroid (i.e. ε is reduced), the less significant are the interactions between the bodies, i.e. the normalized magnitude of the force is close to 1 and its phase is very low.

Our results are in qualitative agreement with the experimental findings of Bathellier *et al.* (2005) for the coupling between pairs of trichobothria. They found that the lower the frequency of oscillations, the thicker the region of viscous coupling. A quantitative comparison of our calculations with their measurements is impossible, as we are solving a resistance problem (the velocity of the body is given and the forces and moments are to be found) while they describe a situation of a mobility problem (the forces and moments are given and the motion of the body is to be determined).

The local flow field, as reflected by the values of the intensities of singularities, is also a result of those opposite trends; thus, for low frequencies of oscillations and quite close bodies we found that the minimum intensity is located at the centre of the body (where the presence of the other spheroid is most helpful), while for high frequencies or when the bodies are separated by a great distance it is the maximum intensity that was attained at the centre of the body (where the other body makes it most difficult to move).

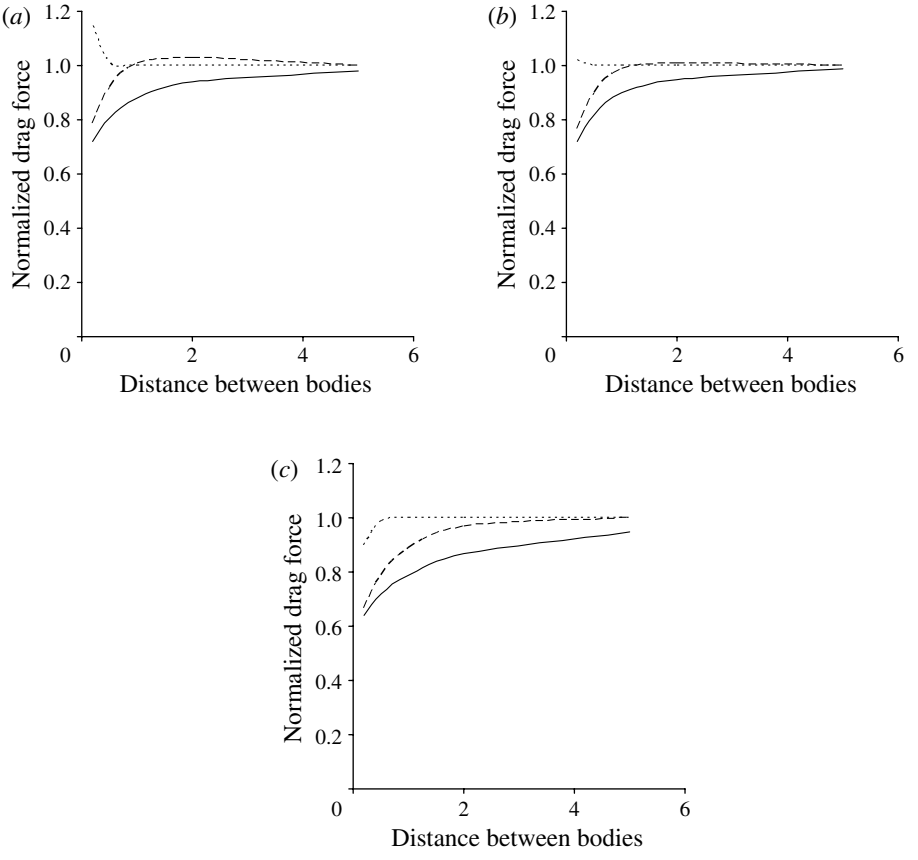

FIGURE 8. The magnitude of the drag exerted by a slender spheroid ($\varepsilon = 0.02$) that is d body half-lengths apart from a similar spheroid in oscillatory motion. Solid line, $\lambda = 0.1(1 - \mathrm{i})$; dashed line, $\lambda = (1 - \mathrm{i})$; dotted line, $\lambda = 10(1 - \mathrm{i})$. The drag is normalized by that exerted by a similar isolated spheroid. Motion is along the (*a*) normal direction, (*b*) tangential direction, (*c*) bi-normal direction.

3.2.2. *A row of parallel spheroids*

The interplay between the viscous character of the slow flow and the inertial effects that stem from the unsteadiness, demonstrated above for the case of two adjacent bodies, induces complicated situations when many bodies are involved. The trends found above become more significant when the number of rods in the row increases. Specifically, as long as the motion is in the bi-normal direction (one spheroid moves 'behind' the other), there is a considerable gain from the clustering of the rods and the overall force needed to move the row is quite low, e.g. 50 rods move with a drag needed for the motion of just 25 isolated rods even when they are not in close proximity ($d = 50\varepsilon$) and the frequency is high ($\lambda = 3(1 - \mathrm{i})$). But for the same parameter values and motion along the normal direction (one spheroid moves in parallel to the other), this row of rods involves a drag force that is higher than that needed for the locomotion of all its components when isolated; see table 3. In contrast to the situation found in Stokes flow, where increasing the number of rods in a row always means a lower drag force exerted by each rod (Barta & Weihs 2006), here extending the row of rods might improve the efficacy of locomotion, or

	$\lambda = 0$		$\lambda = 0.3(1 - \mathrm{i})$		$\lambda = 3(1 - \mathrm{i})$	
	$d = 10\varepsilon$	$d = 50\varepsilon$	$d = 10\varepsilon$	$d = 50\varepsilon$	$d = 10\varepsilon$	$d = 50\varepsilon$
e_n direction	4.4	10.1	$5.44\mathrm{e}^{-0.18\mathrm{i}}$	$16.26\mathrm{e}^{-0.31\mathrm{i}}$	$20.95\mathrm{e}^{-0.75\mathrm{i}}$	$62.25\mathrm{e}^{-0.26\mathrm{i}}$
e_b direction	3.1	6.5	$3.47\mathrm{e}^{-0.11\mathrm{i}}$	$8.80\mathrm{e}^{-0.21\mathrm{i}}$	$7.25\mathrm{e}^{-0.40\mathrm{i}}$	$24.70\mathrm{e}^{-0.39\mathrm{i}}$
e_t direction	5.0	12.5	$5.75\mathrm{e}^{-0.12\mathrm{i}}$	$17.62\mathrm{e}^{-0.21\mathrm{i}}$	$12.98\mathrm{e}^{-0.41\mathrm{i}}$	$40.08\mathrm{e}^{-0.24\mathrm{i}}$

TABLE 3. The overall drag forces exerted on a row normalized by the drag on a single, isolated spheroid. The row consists of 50 spheroids; $\varepsilon = 1/300$.

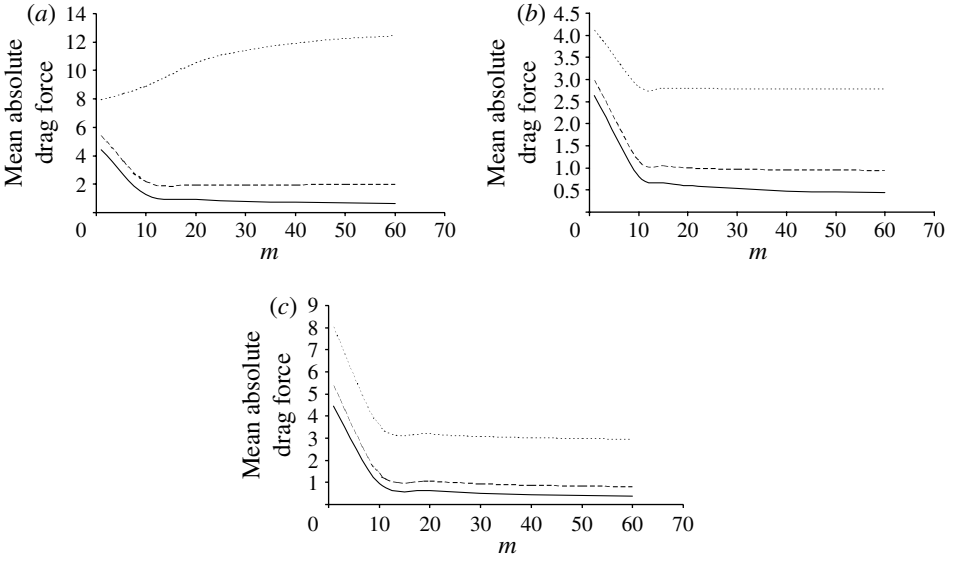

FIGURE 9. The mean drag force exerted by a rod in a row of m spheroids with gaps of 0.1 body half-lengths; $\varepsilon = 0.01$; solid line, $\lambda = 0.1(1 - \mathrm{i})$; dashed line, $\lambda = (1 - \mathrm{i})$; dotted line, $\lambda = 5(1 - \mathrm{i})$. Motion is along the ($a$) normal direction, ($b$) tangential direction, (c) bi-normal direction.

the other way around. The direction of motion, the slenderness ratio, the frequency of oscillations, the number of rods and the distances between them all affect the involved drag forces. From figure 9 it is evident that when the frequency is low, the motion of the row is Stokes-like, i.e. the rods are dragged by the flow created by their neighbours (transferred to them via the viscous ambient fluid) and the force they exert is relatively low. This is especially true for motion along the axis that 'connects' their centres (the bi-normal direction). However, for high or even moderate frequencies, the presence of the neighbours can disturb the motion when the row moves along the normal direction, and is only a slight boon for tangential motion. Those effects become more pronounced as the bodies become closer (shorter distance d) or less slender (higher ε) or oscillate with a higher frequency λ.

Note that figure 9 refers to the mean drag force. Each rod exerts its own specific force; those specific forces are quite similar in the central region of the row but might vary significantly (decrease or increase depending on the parameter values) towards the ends of the row.

A different way to estimate the effect of clustering of slender bodies is to examine the degree of leakiness, i.e. does the row of rods act like a continuous sheet and the fluid between the rods actually moves at the same speed as the rods (as occurs in steady Stokes flow: see figure 6 in Barta & Weihs 2006) or are there significant losses in comparison to a full wing? In correlation with our findings regarding the drag forces, the velocities of the fluid between the bodies when the motion is in the bi-normal direction resemble the rods' velocities as the row moves almost like a continuum, even when the frequency of oscillations is quite high; but for motion in the tangential direction and, even more so, for motion in the normal direction, this is not the case. As the frequencies are increased the ambient fluid starts to 'lag' behind, i.e. the magnitude of its velocity decreases and the phase increases. This deviation from coherent motion becomes much more pronounced towards the tips of the spheroids (away from the bodies' centres).

4. A case study

The effect of the oscillatory character of the motion of the body is beautifully demonstrated by modelling the flapping of wings of insects. The thrips family of insects is one of the few families that has been extensively studied, and therefore provides the necessary data for theoretical simulation. The insect has four comb-like wings, which have been shown to produce forces similar to those of solid wings (an experimental study by Sunada *et al.* 2002). With this it can save weight with a minor sacrifice in performance. However, a trial to balance the insect weight and the drag force produced by the wings flapping (the force gained by the effective stroke minus the one spent on the recovery stroke), according to the steady Stokes flow equations, has failed (Barta & Weihs 2004). Here, we recalculate the forces involved by imposing the much more realistic assumption of oscillatory motion.

Using the data supplied by Sunada *et al.* (2002), we concluded the values of the involved geometrical parameters; specifically, the wing span is 8.1×10^{-4} m, the length of the rods, l, equals 1.5×10^{-4} m and $\varepsilon = 5 \times 10^{-3}$. An average wing is composed of about 50 bristles (rods), and thus we get a spacing, d, between the rods of 21.5ε. The frequency of the flapping is about 200 Hz. In fact the motion is composed of two different phases: the effective stroke (ES), where the motion of the rods is normal to their long axis and is fast (velocity U), and the recovery stroke (RS), where the motion is considerably slower (velocity V) and along the tangential direction. In both phases the velocity of the rods increases linearly from almost zero for the first rod (the one closest to the body of the insect) to its maximum (U or V) for the farthest rod. Henceforth we determine the probable velocities and frequencies for the two phases of motion. The overall distance that the rods cover in each cycle of motion (i.e. within 1/200 of a second) is equal to twice the angle of attack (measured to be about sixty degrees) multiplied by the wing span. Therefore we write

$$1/200 = 8.1 \times 10^{-4}(2\pi/3)(1/U + 1/V). \tag{4.1}$$

As far as we know, the ratio between the velocities U and V has not been measured for thrips. Here we have assumed a ratio of 3, which reflects the situation in other species. (For example, see the report by Blake & Sleigh 1974 on the duration ratio for the two phases of stroke that varies from 1.2 in Opalina to 4 in Paramecium and in Pleurobrachia; Fry, Sayaman & Dickinson 2005 found a ratio of 1.2 in Drosophila.) It induces (after substitution in (4.1)) velocities $U = 1.36$ m s^{-1} and $V = 0.45$ m s^{-1} or frequencies of 801.67 s^{-1} and 265.26 s^{-1} for the ES and RS respectively. Equations

(3.1), (3.2) and (3.3) are solved for $m = 51$ rods with λ values of $0.76(1 - \mathrm{i})$ and $0.44(1 - \mathrm{i})$ for the two phases (calculated based on the above frequencies, a characteristic length, dl, of half the body length, and kinematic viscosity of air known to be about 15.7×10^{-6} m^2 s^{-1} at room temperature). The resulting Stokeslet intensities are incorporated in (2.11) to yield the force produced by the motion of each rod. All rods together in the four wings of the insect produce a net drag of magnitude 6.44×10^{-7} kg m s^{-1} in the effective stroke, from which one has to subtract the force required to bring the wing back to its starting position (the recovery stroke), which is equal to 0.87×10^{-7} kg m s^{-1}, meaning that the net gained force of the flapping wings is about 5.6×10^{-7} kg m s^{-1}, a value that almost exactly balances the weight of the thrips (5.9×10^{-7} kg m s^{-1} by Sunada *et al.* 2002).

Implementing the steady-state Stokes equations induced a net force that was significantly lower than the required force and could not explain the hovering of thrips, while here, under the oscillatory assumption, there is an almost perfect balance between the exerted force and the weight, especially when one takes into account the many sources of inaccuracies involved with the data used. Those inaccuracies are mainly differences between forewings and hindwings (we used the only available data, which refer to a forewing), neglecting the central wing rod (the one that connects the bases of all the slender bristles and that exerts its own force), inaccuracy due to the unknown ratio between the velocities U and V, as well as unknown exact values of the angle of attack and the geometrical data concerning the rods.

The difference between the steady solutions and the present one is attributed mainly to the difference found above (see table 3) between the effects of the densely packed row of bodies on its members for motions along normal and tangential directions. While the drag force in normal motion of a 50-rod row in Stokes flow ($\lambda = 0$) is approximately equal to that exerted in motion along the tangential direction, in an oscillatory situation the motion along the normal direction involves much higher forces. Hence the gap between the drag exerted in the effective stroke and the recovery stroke is widened, because it stems not just from the difference in the velocities *per se* but from the different character of the motions in the two phases: the interference due to the presence of adjacent bodies is more significant for motion along the normal direction.

5. Discussion

The flow field in the vicinity of either an isolated slender body or a row of such bodies moving in a time-dependent fashion within a viscous fluid is found by slender-body theory with utilization of singular fundamental solutions for oscillatory, viscous flow. Both the local flow field and the global drag forces involved are determined with relatively little computational effort for a wide range of parameter values (any frequency of oscillations as long as the bodies have a slenderness ratio lower than 0.1 and the spacing between their axes is higher than 5 diameters). A relation between the singularities' intensities is determined so as to make the inaccuracies which are inherent to the method of solution (induced velocity with circumferential variations on the body surface) cause errors no higher than those induced in the steady-state situation (at most a few per cent: Barta & Weihs 2006).

Trends that were previously found to be valid for a non-slender body in oscillatory motion, namely that (*a*) eddies evolve, expand and then disappear in the vicinity of the moving body, (*b*) the singularities' strength is maximal at the centre of the body and decreases towards its ends, (*c*) higher frequency of oscillations leads to higher drag

force, and (*d*) the effect of the oscillations is more pronounced in motion normal to the axis, have been established for the case of a slender body, but the effect of the oscillations was found to be less significant as the body becomes more slender.

In addition, we dealt with multiple bodies configurations and concluded the following.

(*a*) Adjacent slender bodies help each other (i.e. the drag force they exert is lower than that exerted by an isolated body) when moving together in the bi-normal direction, but might disturb each other and induce a higher drag force when motion is in the normal direction. Motion in the tangential direction is somewhere between those two cases.

(*b*) In contrast to the situation in steady states, here the effect of extending a row of bodies is not necessarily monotonic, i.e. a larger row of bodies might be a benefit or a burden in accordance with the direction of motion, slenderness ratio, frequency of flapping and spacing between the bodies.

The unsteady effects proved to be more crucial for a system of multiple bodies than for an isolated body. This can be demonstrated by comparing the results of tables 1 and 3: increasing the value of λ from 0 to $3(1-\mathrm{i})$ leads to an increase of the drag force by factors of $\sim$1.3 and 1.5 for motions along the tangential and normal directions, respectively, for an isolated spheroid, but induces an increase by factors of 2.3, 2.6 and 4.8 for the mean drag force involved in motions in the bi-normal, tangential and normal directions, respectively, for a row of 50 spheroids. Hence, even at low frequencies of oscillations the time-dependent character of a creeping flow cannot be ignored when several adjacent bodies are concerned. Thus, the motion of ciliated bodies or bristled wings (both composed of arrays of densely packed 'rods') was shown here to be highly affected by the oscillatory situation, proving the well-known fact (Sane & Dickinson 2002) that quasi-steady estimates grossly underestimate the magnitude of the mean drag coefficient of flapping wings.

This paper is a step towards a realistic description of the motion of slender bodies within a viscous fluid. Since our method is applicable to any given motion of bodies (or ambient flow field), to any slender body (as long as it has a circular cross-section) and to a wide range of frequencies of oscillations, it is non-specific and might be relevant to quite a few situations. Many solutions that have been previously formulated might serve as a first approximation, but are inadequate for realistic situations. This is either due to the inaccuracies involved (here, as shown in tables 1 and 2, we found that the shape of the body, or its slenderness ratio, has a tremendous effect on the solution, so deduction from known solutions for almost spherical bodies to a slender body will not yield an acceptable estimate) or due to the high computational effort involved (as in the boundary integral methods).

The method developed here may be extended in a straightforward manner to the case of a matrix of rods (instead of a row) in order to simulate the locomotion of micro-organisms with a pseudo-rectangular body covered with cilia, described by Brennen & Winet (1977). Another straightforward extension is a distribution of oscillatory rotlets in order to account for a rotational movement. One of the most interesting simulations would be of an array of cilia with two planar waves, one travelling along the axis of each cilium and the other across the row. As long as the oscillations are coherent (i.e. all rods have the same frequency) our method is valid and may cope with a detailed simulation of the locomotion of micro-organisms, previously dealt with by rough models (e.g. the envelope model: see Blake & Sleigh 1974).

The author is indebted to Professor Danny Weihs for fruitful discussions regarding the flapping of insects.

REFERENCES

BARTA, E. & LIRON, N. 1988 Slender body interactions for low Reynolds numbers. Part II. Body–body interactions. *SIAM J. Appl. Maths* **48**, 1262–1280.

BARTA, E. & WEIHS, D. 2004 Flapping comb-wings in Stokes flow. Report no. 2, Project no. 160036, Faculty of Aerospace Engineering, Technion.

BARTA, E. & WEIHS, D. 2006 Creeping flow around a finite row of slender bodies in close proximity. *J. Fluid Mech.* **551**, 1–17.

BATHELLIER, B., BARTH, F. G., ALBERT, J. T. & HUMPHREY, J. A. C. 2005 Viscosity-mediated motion coupling between pairs of trichobothria on the leg of the spider *Cupiennius salei*. *J. Compar. Physiol.* A **191**, 733–746.

BLAKE, J. R. & SLEIGH, M. A. 1974 Mechanics of ciliary locomotion. *Biol. Rev.* **49**, 85–125.

BRENNEN, C. & WINET, H. 1977 Fluid mechanics of propulsion by cilia and flagella. *Annu. Rev. Fluid Mech.* **9**, 339–398.

CHEER, A. Y. L. & KOEHL, M. A. R. 1987 Paddles and rakes: fluid flow through bristled appendages of small organisms. *J. Theor. Biol.* **129**, 17–39.

CHWANG, A. T. & WU, T. Y. 1975 Hydromechanics of low-Reynolds-number flow. Part 2. Singularity method for Stokes flow. *J. Fluid Mech.* **67**, 787–815.

CLARKE, R. J., JENSEN, O. E., BILLINGHAM, J. & WILLIAMS, P. M. 2006 Three-dimensional flow due to a microcantilever oscillating near a wall: an unsteady slender-body analysis. *Proc. R. Soc.* A **462**, 912–933.

D'ELÍA, J., BATTAGLIA, L., SARRAF, S. & CARDONA, A. A boundary element method for oscillating Stokes flow at low frequencies around a rigid body. A boundary element method for oscillating Stokes flow at low frequencies around a rigid body. 2010 In *Mecánica Computacional*, vol. XXIX (ed. E. Dvorkin, M. Goldschmit & M. Storti).

DUDLEY, R. 2000 *The Biomechanics of Insect Flight: Form, Function, Evolution*. Princeton University Press.

ELLINGTON, C. P. 1984 The aerodynamics of hovering insect flight. Part I. The quasi-steady analysis. *Phil. Trans. R. Soc. Lond.* B **305**, 1–15.

FENG, J. & JOSEPH, D. D. 1995 The unsteady motion of solid bodies in creeping flows. *J. Fluid Mech.* **303**, 83–102.

FRY, S. N., SAYAMAN, R. & DICKINSON, M. H. 2005 The aerodynamics of hovering flight in Drosophila. *J. Expl Biol.* **208**, 2303–2318.

GRAY, J. 1928 *Ciliary Movement*. Cambridge University Press.

JOHNSON, R. E. 1980 An improved slender-body theory for Stokes flow. *J. Fluid Mech.* **99**, 411–431.

KIM, S. & KARRILA, S. J. 1991 *Microhydrodynamics: Principles and Selected Applications*. Butterworth-Heinemann.

KOHR, M. 2003 An indirect boundary integral method for an oscillatory Stokes flow problem. *IJMMS* **47**, 2961–2976.

LAWRENCE, C. J. & WEINBAUM, S. 1986 The force on an axisymmetric body in linearized, time-dependent motion: a new memory term. *J. Fluid Mech.* **171**, 209–218.

LAWRENCE, C. J. & WEINBAUM, S. 1988 The unsteady force on a body at low Reynolds number: the axisymmetric motion of a spheroid. *J. Fluid Mech.* **189**, 463–489.

LIRON, N. & BARTA, E. 1992 Motion of a rigid particle in Stokes flow: a new second-kind boundary-integral equation formulation. *J. Fluid Mech.* **238**, 579–598.

LOEWENBERG, M. 1994 Axisymmetric unsteady Stokes flow past an oscillating finite-length cylinder. *J. Fluid Mech.* **265**, 265–288.

POZRIKIDIS, C. 1989*a* A singularity method for unsteady linearized flow. *Phys. Fluids* A **1** (9), 1508–1520.

POZRIKIDIS, C. 1989*b* A study of linearized oscillatory flow past particles by the boundary-integral method. *J. Fluid Mech.* **202**, 17–41.

SANE, S. P. & DICKINSON, M. H. 2002 The control of flight force by a flapping wing: lift and drag production. *J. Expl Biol.* **204**, 2607–2626.

SHATZ, L. F. 2004 Singularity method for oblate and prolate spheroids in Stokes and linearized oscillatory flow. *Phys. Fluids* **16** (3), 664–677.

SMITH, S. H. 1997 Slow oscillatory Stokes flow. *Q. Appl. Math.* **55**, 1–22.

STOKES, G. G. 1851 On the effect of the internal friction of fluids on the motion of pendulum. *Trans. Camb. Phil. Soc.* **9**, 8.

SUNADA, S., TAKASHIMA, H., HATTORI, T., YASUDA, K. & KAWACHI, K. 2002 Fluid-dynamic characteristics of a bristled wing. *J. Expl Biol.* **205**, 2737–2744.

TAYLOR, G. K. 2001 Mechanics and aerodynamics of insect flight control. *Biol. Rev. Camb. Phil. Soc.* **76**, 449–471.

TSAI, C. C., YOUNG, D. L., FAN, C. M. & CHEN, C. W. 2006 MFS with time-dependent fundamental solutions for unsteady Stokes equations. *Engng Anal. Bound. Elem.* **30**, 897–908.

WEIHS, D. & BARTA, E. 2008 Comb wings for flapping flight at extremely low Reynolds numbers. *AIAA J.* **46** (1), 285–288.

ZUSSMAN, E., YARIN, A. L. & WEIHS, D. 2002 A micro-aerodynamic decelerator based on permeable surfaces of nanofibre mats. *Exp. Fluids* **33**, 315–320.